Electrocatalysis

Deutsche Ausgabe: DOI: 10.1002/ange.201713003
Internationale Ausgabe: DOI: 10.1002/anie.201713003

Densely Packed, Ultra Small SnO Nanoparticles for Enhanced Activity and Selectivity in Electrochemical CO_2 Reduction

*Jun Gu, Florent Héroguel, Jeremy Luterbacher, and Xile Hu**

Abstract: *Controlling the selectivity in electrochemical CO_2 reduction is an unsolved challenge. While tin (Sn) has emerged as a promising non-precious catalyst for CO_2 electroreduction, most Sn-based catalysts produce formate as the major product, which is less desirable than CO in terms of separation and further use. Tin monoxide (SnO) nanoparticles supported on carbon black were synthesized and assembled and their application in CO_2 reduction was studied. Remarkably high selectivity and partial current densities for CO formation were obtained using these SnO nanoparticles compared to other Sn catalysts. The high activity is attributed to the ultra-small size of the nanoparticles (2.6 nm), while the high selectivity is attributed to a local pH effect arising from the dense packing of nanoparticles in the conductive carbon black matrix.*

Electrochemical reduction of CO_2 to form carbon-based fuels and chemicals has been widely proposed for the storage and utilization of intermittent renewable energies such as solar and wind.[1] However, two major deficiencies have prevented CO_2 electroreduction from becoming a viable technology: energy inefficiency owing to large overpotentials, and poor selectivity leading to separation issues. Therefore, there is tremendous interest in developing active and selective electrocatalysts for CO_2 reduction. In terms of electrochemical activity, noble-metal catalysts rank the best.[2] Among non-noble metal catalysts, Sn-based catalysts stand out.[3,4] However, the major CO_2 reduction product using Sn catalysts is formate ($HCOO^-$), and CO is generated only in a small amount.[5] Unlike its acidic form, formic acid which is a high-value chemical, formate has no obvious usage and is difficult to separate and convert into other high-value products without adding costly processes. CO, on the other hand, is a highly desirable product as it is a gas that can be easily separated and further converted into fuels and bulk chemicals at a large scale through existing chemical technologies. Achieving high activity and selectivity for CO formation on a non-precious catalyst such as Sn is therefore a notable goal with practical relevance.

The CO_2 electroreduction performance of Sn based catalysts developed recent years is summarized in the Supporting Information, Figure S4. Modulation of size, shape, and composition (metal, oxide, or sulfide) of monometallic Sn catalysts is effective to achieve high formate formation activity, but these approaches cannot improve CO formation performance.[5a–d] Until now, cooperative promotion is required to enhance CO formation on Sn-based catalysts. For example, Cu-Sn bimetallic catalysts are reported to favor CO formation;[6] however, Cu also acts as possible catalytic sites. Herein we report a new strategy that leads to unprecedented activity and selectivity for CO formation among monometallic Sn catalysts. Key to this performance are the ultra-small size of catalyst nanoparticles and their dense packing in a conductive matrix, which lead to a high density of active site and a local pH effect that favors the formation of CO over formate.

To prepare densely packed ultra-small Sn nanoparticles, we considered to derive them from a suitable tin oxide. Sn is a low melting-point metal, and thus many synthetic methods for nanoparticles that involve thermal treatments are more adapted for tin oxides than for Sn.[7] Moreover, previous work showed that oxide-derived metal catalysts can have higher roughness and surface areas, which is beneficial for CO_2 reduction.[8] We chose SnO because unlike SnO_2, it has not been explored as precursors for catalysts for CO_2 electroreduction. Figure 1a shows the synthetic strategy of carbon-black-supported SnO (SnO/C) as the precatalyst. A composite of carbon black and Sn^{II} oxalate (SnC_2O_4/C; Supporting Information, Figure S5) was first prepared by co-precipitation. Pyrolysis of SnC_2O_4/C at 400 °C in an N_2 atmosphere then yielded SnO/C. For comparison purpose, precatalysts based on SnO_2 (SnO_2/C) and Sn nanoparticles (Sn/C) were also fabricated. SnO_2/C was prepared similarly to SnO/C, except that the pyrolysis was conducted in air (Figure 1a). Sn/C was prepared by reducing $SnCl_2$ with $NaBH_4$ in the presence of carbon black.

The X-ray diffraction (XRD) patterns confirm the crystallographic phase of SnO/C (Figure 1b), SnO_2/C and Sn/C (Supporting Information, Figure S6), and the broad diffraction peaks of SnO/C and SnO_2/C indicate the nanosized features of SnO and SnO_2. The loadings of SnO, SnO_2, and Sn in the composites determined by thermal gravity analysis (TGA) in air were 46.0%, 49.2%, and 49.3%, respectively (Supporting Information, Figure S7). X-ray photoelectron spectroscopy (XPS) analyses (Supporting Information, Figure S8 and Table S2) show that the surfaces of Sn and SnO were partially oxidized to form SnO_2 species when exposed to

[*] Dr. J. Gu, Prof. Dr. X. L. Hu
Laboratory of Inorganic Synthesis and Catalysis, Institute of Chemical Sciences and Engineering
Ecole Polytechnique Fédérale de Lausanne (EPFL)
1015 Lausanne (Switzerland)
E-mail: xile.hu@epfl.ch
Dr. F. Héroguel, Prof. Dr. J. Luterbacher
Laboratory of Sustainable and Catalytic Process, Institute of Chemical Sciences and Engineering
Ecole Polytechnique Fédérale de Lausanne (EPFL)
1015 Lausanne (Switzerland)
Supporting information and the ORCID identification number(s) for the author(s) of this article can be found under: https://doi.org/10.1002/anie.201713003.

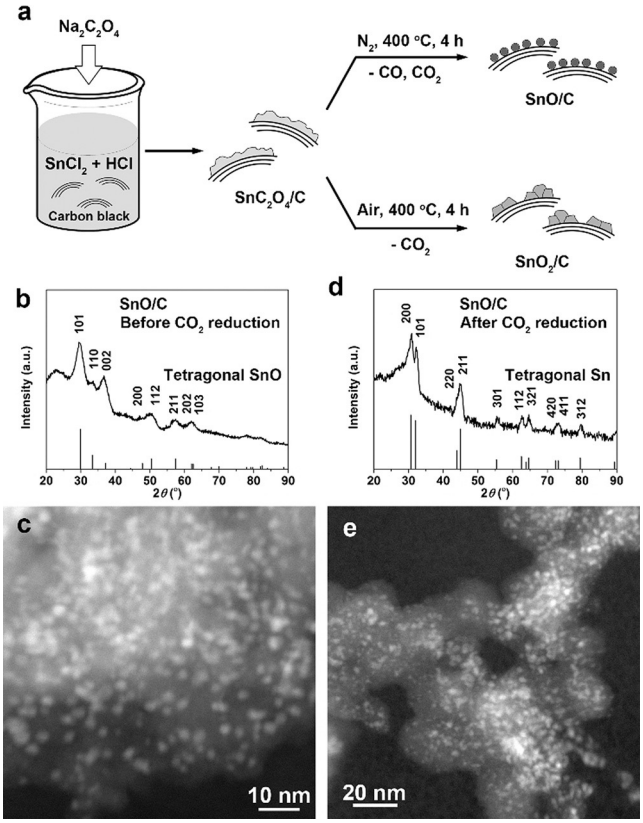

Figure 1. a) Synthetic strategies of SnO/C and SnO_2/C. b),d) XRD patterns and c),e) HAADF-STEM images of SnO/C before (b,c) and after (d,e) electrolysis at −0.66 V vs. RHE in CO_2 saturated 0.5 M $KHCO_3$ electrolyte for 1800 s. Vertical lines in (b) and (d) are standard diffraction patterns of tetragonal SnO (JCPDS no. 06-0395) and tetragonal Sn (JCPDS no. 04-0673), respectively.

air. The high-angle annular dark-field scanning transmission electron microscopy (HAADF-STEM) images of SnO/C are shown in the Figure 1c and the Supporting Information, Figure S9a. These images reveal ultra-small SnO nanoparticles as bright dots with an average size of 2.6 ± 0.4 nm, homogeneously dispersed on the carbon black substrate, which appears as a gray background. The interparticle distance is about 4 nm. High-resolution transmission electron microscopy (HRTEM) image reveals the single-crystalline nature of SnO nanoparticles (Supporting Information, Figure S9b). On the other hand, SnO_2 nanoparticles in SnO_2/C (Supporting Information, Figure S10) have an average size of 5.0 ± 0.9 nm, twice as large as SnO, and aggregation occurs to some degree. Sn particles in Sn/C have a wide size distribution of 30 to 200 nm (Supporting Information, Figure S11).

The post-catalytic characterizations of SnO/C after electrolysis at −0.66 V versus reversible hydrogen electrode (RHE) in CO_2 saturated 0.5 M $KHCO_3$ electrolyte for 1800 s are shown in Figure 1d,e. The applied potential is much more negative than the reduction potential of SnO and SnO_2, that is −0.10 V and −0.09 V vs. RHE, respectively.[9] The XRD pattern of SnO/C after electrolysis indeed only shows the peaks of metallic Sn. However, peaks of SnO_2 still exist with those of metallic Sn in the XRD pattern of SnO_2/C after electrolysis (Supporting Information, Figure S13a), indicating incomplete reduction, which is probably due to the larger size and aggregation. After electrolysis, Sn nanoparticles derived from SnO maintained a similar size (3.0 ± 0.9 nm), high dispersity, and single-crystalline nature as their SnO precursors (Figure 1e; Supporting Information, Figure S12). Although ultra-small Sn nanoparticles should be easily oxidized when exposed to air, the Nafion binder in the catalyst seems to prevent this oxidation. In contrast, SnO_2-derived nanoparticles after electrolysis have a much larger size (8.3 ± 1.8 nm), polycrystalline nature, and suffer from aggregation (Supporting Information, Figure S13b,c).

The catalytic activity and selectivity of SnO/C, SnO_2/C, and Sn/C in CO_2 electroreduction were tested in CO_2 saturated 0.5 M $KHCO_3$ electrolyte. H_2, CO, and formate were the only products detected by gas chromatography and ^{1}H NMR spectroscopy. SnO/C showed the highest current density in both linear sweep voltammetry (LSV) curves (Supporting Information, Figure S14) and chronoamperometry (CA) curves (Supporting Information, Figure S15). An induction period was observed for every pre-catalyst in the CA curves, which is most likely attributed to the reduction of tin oxides to Sn. SnO/C showed good stability in a 1-day CA test at −0.66 V vs. RHE (Supporting Information, Figure S16), with a stable current density about 13 mA cm^{-2} and the Faraday efficiency of CO constantly between 30% and 40%. The Faraday efficiency of formate of the one-day electrolysis was 36%.

The potential-dependent Faraday efficiency (Figure 2a–c) and partial current density (Figure 2d–e) for CO and formate formation of the SnO/C, SnO_2/C and Sn/C pre-catalysts were then determined. SnO/C shows the highest Faraday efficiency to CO_2 reduction, and more importantly, to CO formation at all applied potentials, which keeps above 20% and has the maximum of 37% at −0.66 V vs. RHE. The partial current density for CO formation of SnO/C is about an order of magnitude higher than that of SnO_2/C and Sn/C. At −0.66 V

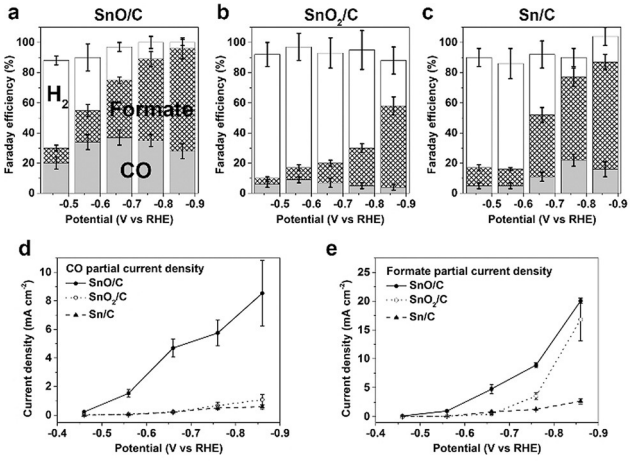

Figure 2. a)–c) Faraday efficiencies of CO (gray), formate (hashed), and H_2 (white) of a) SnO/C, b) SnO_2/C, and c) Sn/C at different applied potentials. d),e) Partial current densities of d) CO and e) formate of SnO/C (solid), SnO_2/C (dotted), and Sn/C (dashed) at different applied potentials.

and −0.86 V vs. RHE, the current density was 4.7 and 8.5 mA cm^{-2}, respectively. The partial current density for formate formation of SnO/C is higher than SnO_2/C and Sn/C as well. As shown in the Supporting Information, Figure S4, the Faraday efficiency and partial current density of CO formation of SnO/C were substantially higher than those of other Sn based catalysts in previous reports.[5] The partial current density of formate formation of SnO/C is also among the highest in Sn-based catalysts.[5]

Since post-catalytic characterization data indicate that SnO and SnO_2 precursors were transformed into metallic Sn during electrolysis, the superior activity and selectivity of SnO/C warrants additional analysis. Compared to SnO_2/C and Sn/C, the Sn nanoparticles derived from SnO/C has a significantly smaller size. As a result, SnO/C possessed a higher surface area, as indicated by the measurements of double-layer capacitances (Supporting Information, Figure S17) and Brunauer–Emmett–Teller (BET) analysis (Supporting Information, Figure S18 and Table S3). However, the less than two-fold increase in surface area cannot account for the more than 10 times higher partial current densities of CO formation on SnO/C.

Nanoparticles with smaller size expose a higher proportion of step and corner sites, which might bind adsorbates stronger than terrace sites. As indicated by the anodic LSV curves in N_2 saturated 0.1 M KOH electrolyte (Supporting Information, Figure S19), the potential for oxidative adsorption of OH^- on SnO/C was more negative than that of the other two samples, revealing a stronger binding to OH group. OH has been considered as a surrogate of $CO_2^{\bullet-}$, while the adsorption energy of $CO_2^{\bullet-}$ is a descriptor of the activity of CO_2 reduction.[5a–c,10] This result implies Sn nanoparticles derived from SnO/C adsorb $CO_2^{\bullet-}$ stronger than those derived from SnO_2/C and Sn/C. The better stabilization of $CO_2^{\bullet-}$ intermediate, probably attributed to the ultra-small particle size, is likely the origin of the higher activity of SnO/C.

However, the size effect cannot explain the high selectivity of SnO/C towards CO formation. In our SnO/C sample, nanoparticles of the SnO pre-catalyst, and the actual Sn catalyst, are densely distributed in the carbon matrix. We hypothesized that this dense distribution might affect microscopic diffusion, and thus, influence the CO_2 reduction selectivity.[11] To probe the effect of SnO density, we synthesized another sample of carbon black supported SnO nanoparticles with a lower weight fraction (8.4 %) of SnO (denoted as l-SnO/C). The average size of SnO nanoparticles was 3.0 ± 0.8 nm (Supporting Information, Figure S20), similar to that of SnO/C. As indicated by the averaged nanoparticle-centered radial distribution diagrams of particle density (Supporting Information, Figure S3), the particle density within a short radius of one SnO nanoparticle of SnO/C is significantly higher than that of l-SnO/C. Figure 3a and 3b compare the Faraday efficiencies and partial current densities of CO and formate formation on SnO/C and l-SnO/C, at a similar loading of SnO. Compared to SnO/C, l-SnO/C has a much lower selectivity towards CO formation while favoring formate formation. As the particle sizes of SnO/C and l-SnO/C were similar, the particle density in the carbon black matrix seems to be the main factor affecting the selectivity.

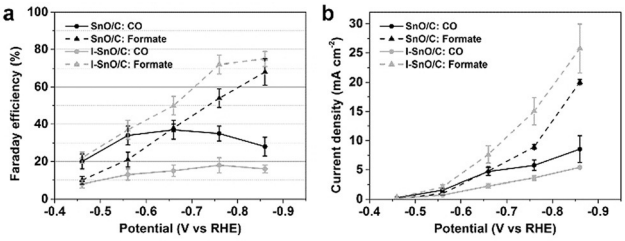

Figure 3. a) Faraday efficiencies and b) partial current densities of CO (solid curves) and formate (dashed curves) of SnO/C (black) and l-SnO/C (gray) at different applied potentials.

It has been observed in previous work[5b,c] that on tin-based catalysts, by applying larger bias, an increase of current density was accompanied by an increase of the Faraday efficiency of CO. High current density, namely higher consuming rate of proton source, leads to a significant raise in local pH value near the catalytic sites, which might be the origin of the increased CO selectivity. In 0.5 M $KHCO_3$ electrolyte, the proton donor was HCO_3^- ($pka = 10.3$).[9] The simulation[12] showed that in the electrolyte containing 0.5 M $KHCO_3$, the local pH value at a flat electrode is about 2 pH units higher than that in bulk electrolyte when the current density is 5 mA cm^{-2}, and this difference increase significantly as the current density increases. We consider that in the catalyst composed of more densely packed nanoparticles, in this case, the SnO/C sample, the local current density around one nanoparticle at a given overpotential is higher, and the local pH value should be higher. If the formation rates of CO and formate show different dependence on the concentration of proton donor, this local pH effect will lead to the variation of the selectivity between CO and formate.

The local pH effect is expected to be more pronounced in electrolytes with weaker buffer capacities.[8c,13] The product distribution of CO_2 reduction on SnO/C in three different electrolytes (0.5 M K_2HPO_4, 0.5 M $KHCO_3$, and 0.5 M KCl) is compared in the Supporting Information, Figure S21. As the buffer capacity of electrolyte decreases from K_2HPO_4 to $KHCO_3$ to KCl, the Faraday efficiency of CO increases gradually. This result supports that a higher local pH effect enhances CO selectivity.

The possible pathways of CO and formate formation on Sn are shown in Figure 4a.[3,6b] For each pathway, if the first step, the single electron transfer to CO_2, is the rate determining step (RDS), the Tafel slop should be 118 mV dec^{-1}. If this step is reversible, followed by a rate-limiting proton transfer from HCO_3^-, the Tafel slop should be 59 mV dec^{-1}.[14,15] As indicated by the Tafel plots of SnO/C (Figure 4b), the Tafel slopes of formate formation is 64 mV dec^{-1}, close to 59 mV dec^{-1}, similar to that reported for other Sn-based catalysts,[4,5a,b] suggesting that the RDS is the protonation of the adsorbed $CO_2^{\bullet-}$. Meanwhile, the Tafel slope of CO formation is 94 mV dec^{-1}, close to 118 mV dec^{-1}, suggesting that the formation rate of CO is more limited by the first single electron transfer step. The Tafel analysis suggests that

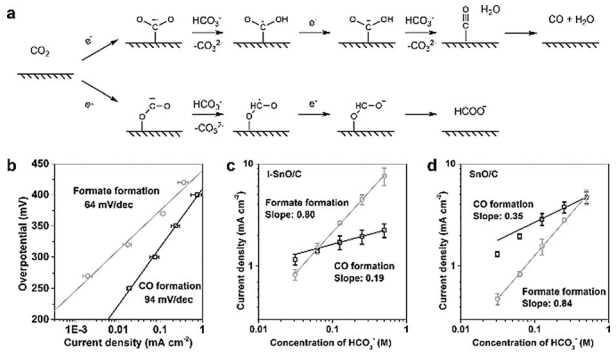

Figure 4. a) Proposed reaction pathways of CO and formate formation on Sn. b) Tafel plots of CO (black) and formate (gray) formation on SnO/C. c),d) Partial current densities of CO (black) and formate (gray) depending on the concentration of HCO_3^- for l-SnO/C (c) and SnO/C (d) at −0.66 V vs. RHE.

the change of local pH will largely change the rate of formate formation, but not CO formation.

To provide further support to the above Tafel analysis, the apparent reaction orders of HCO_3^- in CO and formate formation for l-SnO/C and SnO/C were measured (Figure 4c,d). The reaction order of HCO_3^- in formate formation was about 0.8, which is close to first order. This result agrees with the previous report on nanosized SnO_2/C[5a] and supports that the protonation of adsorbed $CO_2^{\bullet-}$ is the RDS for formate formation. The rate orders of HCO_3^- for CO formation was much smaller, being 0.19 for l-SnO/C and 0.35 for SnO/C. This result agrees with previous studies on Au[15] and Ag[8c] where the rate order of HCO_3^- for CO formation was close to zero. It is consistent with the reduction of CO_2 to $CO_2^{\bullet-}$ being the RDS for CO formation. Based on the reaction orders, a 10-fold increase of the concentration of HCO_3^- will lead to a 4-fold increase in the selectivity of CO over formate. These results indicate that formate formation is greatly disfavored over CO formation when the concentration of proton source is decreased, consistent with the local pH effect proposed above.

Because CO formation also involves protonation (Figure 4a), when the concentration of HCO_3^- is low enough, the protonation step will be slowed down sufficiently to have a comparable rate to the reduction of CO_2 to $CO_2^{\bullet-}$. This analysis gives a possible explanation for the non-zero order of HCO_3^- in CO formation. The higher order of our optimized catalyst, SnO/C than l-SnO/C (which has a lower packing density than SnO/C) suggests that the local concentration of HCO_3^- around SnO/C is lower than around l-SnO/C, again consistent with a higher local pH effect for the more densely packed particles.

In summary, a simple synthetic method has been developed for ultra-small (2.6 nm) SnO nanoparticles densely dispersed in carbon black. These SnO nanoparticles are completely reduced to Sn nanoparticles of similar size and dispersion under conditions employed for CO_2 electroreduction. Compared to other Sn-based catalysts, the SnO/C derived catalyst exhibits remarkably high selectivity and partial current density of CO formation, as well as one of the highest partial current densities of formate formation. The high activity originates from its ultra-small particle size, which enhances $CO_2^{\bullet-}$ absorption, and the high selectivity for CO formation is attributed to a local pH effect arising from the high density of nanoparticles in the conductive carbon black matrix. Local pH increase suppresses formate formation while shows less influence on the formation rate of CO. The tuning of the distribution of nanocatalysts in a conductive matrix might be further exploited as a design strategy for the development of selective CO_2 reduction electrocatalysts.

Acknowledgements

This work is supported by the GAZNAT S.A. through a research project contract with EPFL. We thank Dr. Heron Vrubel (EPFL) for experimental assistance, Dr. Fang Song (EPFL) for electron microscopic characterizations, and Weiyan Ni (EPFL) for XRD measurements. We also thank Prune Hu (Suricate Design) for help with the Table of Contents graphic.

Conflict of interest

The authors declare no conflict of interest.

Keywords: carbon dioxide reduction · electrocatalysis · nanoparticles · particle density · tin oxide

How to cite: *Angew. Chem. Int. Ed.* **2018**, *57*, 2943–2947
Angew. Chem. **2018**, *130*, 2993–2997

[1] a) "Electrochemical CO_2 Reduction on Metal Electrodes": Y. Hori, in *Modern Aspects of Electrochemistry* (Eds.: C. T. Vayenas, R. E. White, M. E. Gamboa-Aldeco), Springer, New York, **2008**, pp. 89–189; b) D. D. Zhu, J. L. Liu, S. Z. Qiao, *Adv. Mater.* **2016**, *28*, 3423–3452.

[2] a) H. Mistry, R. Reske, Z. Zeng, Z.-J. Zhao, J. Greeley, P. Strasser, B. R. Cuenya, *J. Am. Chem. Soc.* **2014**, *136*, 16473–16476; b) Q. Lu, J. Rosen, Y. Zhou, G. S. Hutchings, Y. C. Kimmel, J. G. Chen, F. Jiao, *Nat. Commun.* **2014**, *5*, 3242; c) X. Min, M. W. Kanan, *J. Am. Chem. Soc.* **2015**, *137*, 4701–4708.

[3] Y. Hori, H. Wakebe, T. Tsukamoto, O. Koga, *Electrochim. Acta* **1994**, *39*, 1833–1839.

[4] Y. Chen, M. W. Kanan, *J. Am. Chem. Soc.* **2012**, *134*, 1986–1989.

[5] a) S. Zhang, P. Kang, T. J. Meyer, *J. Am. Chem. Soc.* **2014**, *136*, 1734–1737; b) F. Lei, W. Liu, Y. Sun, J. Xu, K. Liu, L. Liang, T. Yao, B. Pan, S. Wei, Y. Xie, *Nat. Commun.* **2016**, *7*, 12697; c) D. H. Won, C. H. Choi, J. Chung, M. W. Chung, E.-H. Kim, S. I. Woo, *ChemSusChem* **2015**, *8*, 3092–3098; d) F. Li, L. Chen, M. Xue, T. Williams, Y. Zhang, D. R. MacFarlane, J. Zhang, *Nano Energy* **2017**, *31*, 270–277; e) W. Luc, C. Collins, S. Wang, H. Xin, K. He, Y. Kang, F. Jiao, *J. Am. Chem. Soc.* **2017**, *139*, 1885–1893.

[6] a) S. Sarfraz, A. T. Garcia-Esparza, A. Jedidi, L. Cavallo, K. Takanabe, *ACS Catal.* **2016**, *6*, 2842–2851; b) Q. Li, J. Fu, W. Zhu, Z. Chen, B. Shen, L. Wu, Z. Xi, T. Wang, G. Lu, J.-j. Zhu, S. Sun, *J. Am. Chem. Soc.* **2017**, *139*, 4290–4293; c) M. Schreier, F. Héroguel, L. Steier, S. Ahmad, J. S. Luterbacher, M. T. Mayer, J. Luo, M. Grätzel, *Nat. Energy* **2017**, *2*, 17087.

[7] a) T. Kida, T. Doi, K. Shimanoe, *Chem. Mater.* **2010**, *22*, 2662–2667; b) D. Aurbach, A. Nimberger, B. Markovsky, E. Levi, E. Sominski, A. Gedanken, *Chem. Mater.* **2002**, *14*, 4155–4163.

[8] a) Y. Chen, C. W. Li, M. W. Kanan, *J. Am. Chem. Soc.* **2012**, *134*, 19969 – 19972; b) C. W. Li, J. Ciston, M. W. Kanan, *Nature* **2014**, *508*, 504 – 507; c) M. Ma, B. J. Trześniewski, J. Xie, W. A. Smith, *Angew. Chem. Int. Ed.* **2016**, *55*, 9748 – 9752; *Angew. Chem.* **2016**, *128*, 9900 – 9904.
[9] W. M. Haynes, in *CRC Handbook of Chemistry and Physics*, 91st Edition, CRC Press, Boca Raton, FL, **2010**.
[10] A. Salehi-Khojin, H.-R. M. Jhong, B. A. Rosen, W. Zhu, S. Ma, P. J. A. Kenis, R. I. Masel, *J. Phys. Chem. C* **2013**, *117*, 1627 – 1632.
[11] a) H. Mistry, F. Behafarid, R. Reske, A. S. Varela, P. Strasser, B. Roldan Cuenya, *ACS Catal.* **2016**, *6*, 1075 – 1080; b) Y. Yoon, A. S. Hall, Y. Surendranath, *Angew. Chem. Int. Ed.* **2016**, *55*, 15282 – 15286; *Angew. Chem.* **2016**, *128*, 15508 – 15512.
[12] N. Gupta, M. Gattrell, B. Macdougall, *J. Appl. Electrochem.* **2006**, *36*, 161 – 172.
[13] M. Ma, K. Djanashvili, W. A. Smith, *Angew. Chem. Int. Ed.* **2016**, *55*, 6680 – 6684; *Angew. Chem.* **2016**, *128*, 6792 – 6796.
[14] E. Gileadi, in *Electrode Kinetics for Chemists, Chemical Engineers and Materials Scientists*, Wiley-VCH, Weinheim, **1993**.
[15] A. Wuttig, Y. Yoon, J. Ryu, Y. Surendranath, *J. Am. Chem. Soc.* **2017**, *139*, 17109 – 17113.

Manuscript received: December 18, 2017
Accepted manuscript online: January 22, 2018
Version of record online: February 14, 2018

